7.2

HEAT TRANSFER IN MELT PONDS

Eric D. Skyllingstad* and Clayton Paulson
Oregon State University, Corvallis,
Oregon

1. INTRODUCTION

One of the main difficulties in modeling climate change is the accurate prediction of physical processes that change the radiative balance of the coupled atmosphere-ocean system. For example, processes that control ice and snow coverage directly affect the radiative budget by setting the amount of solar radiation reflected back into space by the earth's surface albedo. If climate warming causes a decrease in surface ice and snow coverage and the corresponding surface albedo, then the greater absorption of solar radiation could accelerate the increase in global temperatures. This nonlinear interaction is commonly referred to as the "ice-albedo feedback," and has been identified as a key component of the earth's climate system (Untersteiner, 1990).

A primary motivation for the year-long Surface Heat Budget of the Arctic Ocean (SHEBA) Project was to gain a better understanding of the ice-albedo feedback by combining detailed measurements of the sea ice characteristics with extensive surface flux measurements. A significant finding from the SHEBA experiment was the observation that melt pond albedo has a critical role in determining the overall ice surface characteristic and was probably more important for solar absorption during SHEBA than open leads.

In general, our understanding of melt ponds is not very extensive. Basic aspects of melt pond evolution have not been measured, such as lateral bottom melt rates, internal heat exchange, and solar absorption. In this paper, preliminary experiments are presented that examine how an idealized lead responds to solar heating and wind forced mixing. A large-eddy simulation (LES) model is used to conduct these experiments for square melt pond configurations designed to simplify the interpretation of the model results.

* *Corresponding author address*: Eric Skyllingstad, 104 COAS Admin Bldg, Oregon State University, Corvallis, OR, 97331; e-mail: skylling@coas.oregonstate.edu.

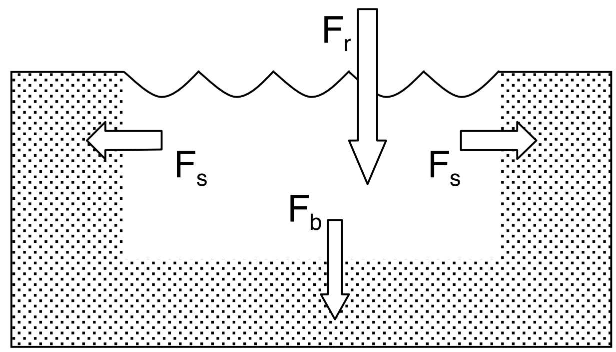

Figure 1. Schematic diagram of a simulated square melt pond showing flux of solar radiation, F_r, edge melting flux, F_s, and bottom melting flux, F_b.

An example of the simulated melt pond configuration is shown in Fig. 1. We can partition the primary pond fluxes between the side and bottom surfaces,

$$F_r L^2 = F_s 4Ld + F_b L^2 \tag{1}$$

where F_r is the total absorbed solar radiation, F_s is the heat flux used in melting the side of the pond, F_b is the heat flux used in melting the pond bottom, L is the pond width, and d is the pond depth. Growth of the pond depends on a number of factors including the partition of energy between the bottom and side melting, dependence of solar absorption on the depth of the pond, and the bottom reflection of solar radiation reaching the pond bottom.

We can use (2) to evaluate basic characteristics of pond behavior. For example, if we assume a fully turbulent pond with minimal conductive heat flux in the ice and nearly instantaneous heat transfer, then we would expect

F_s and F_b to be roughly equal, in which case (1) can be rearranged

$$\frac{F_{melt}}{F_r} = \frac{L}{(4d + L)} \qquad (2)$$

where F_{melt} is the average ice melting flux. Equation (3) suggests that F_{melt} should approach F_r as the pond radius increases since d becomes much smaller than r. To test this idea, we apply observations from Perovich et al. (2003) showing d = ~0.2 when the L was ~5 m and d = ~0.4 m, when L was ~10 m. Using (2) and the observed pond dimensions, we calculate that the melting flux would be roughly constant at 0.862 of the incoming radiative flux regardless of the pond size.

With this simple model, we cannot explain why the flux ratio is a constant. In actual ponds F_b and F_s are probably not equal because of variable pond circulations and possible stratification. In addition, the shape of the pond is typically complex so the idealized pond will not adequately cover ponds having channels and corrugated side walls. Most importantly, assuming side and bottom melt rates are equal does not take into account the increase in F_r that would accompany increased depth and greater water mass for radiative absorption, which is a key aspect of the ice-albedo feedback. Here, the LES model is used to examine a number of these factors, focusing specifically on the role of wind stress and pond size on controlling edge melting.

2. Experiment Design

Simulations were conducted using the LES model described in Skyllingstad et al. (2003) for a confined domain as shown schematically in Fig. 1. Square melt ponds were simulated using a grid with 248 grid points in the horizontal directions and 26 points in the vertical. Two melt pond sizes were considered by applying a uniform grid spacing of 0.025 and 0.05, yielding a small melt pond 0.65 m deep and 6.2 m wide, and a large melt pond 1.3 m deep and 12.4 m wide.

Initial conditions were selected with a goal of reaching an equilibrium condition whereby melt fluxes balance the incoming solar radiation with minimal change in the pond internal temperature. Achieving this goal required a number of test simulations using different initial temperature values depending on the wind forcing and pond size. Initial melt water salinity was set to 2 psu and ice salinity to 4 psu. Simulation duration ranged from ~4 to 8 hrs, depending on the time required to reach near steady-state. We consider three cases; the first using the large pond configuration with a wind stress of 0.05 N m^{-2}, the second using the small pond with wind stress of 0.05 N m^{-2}, and the third using the small pond with no wind forcing. Solar radiation is fixed at 240 W m^{-2}, with a –30 W m^{-2} sensible and latent flux imposed at the pond surface. Radiative absorption was modeled using an empirical formula based on lead measurements and assuming a pond bottom albedo of 0.7.

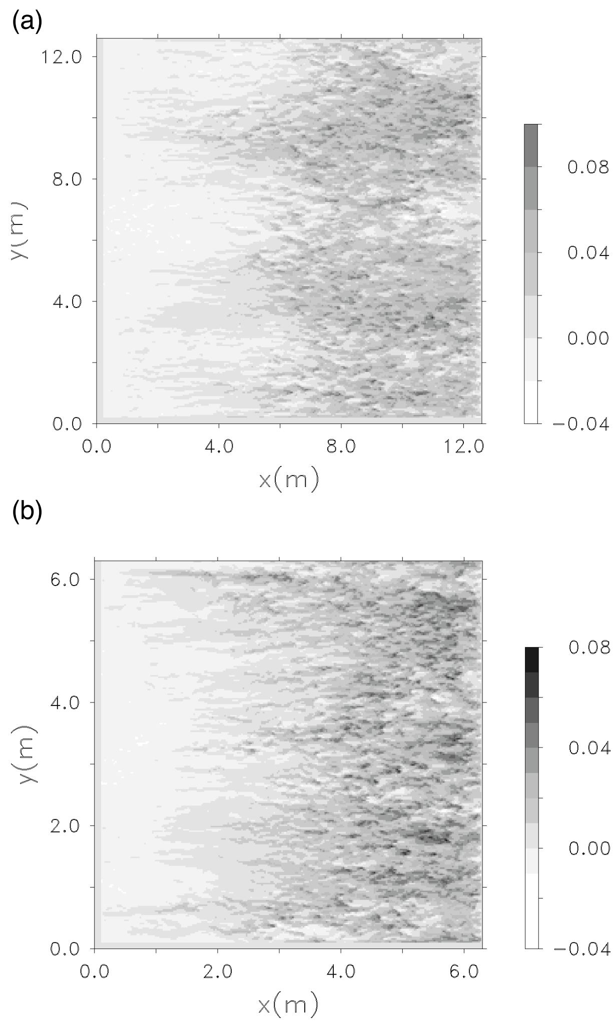

Figure 2. Current speed (m s^{-1}) in the down wind direction (left to right) for the (a) large pond simulation at a depth of 0.2 m and (b) small pond simulation at a depth of 0.1 m. Note that the velocity scaling is different in each case.

3. Results

We begin the analysis of the three simulations by showing circulation plots for the two wind driven cases (Fig. 2). In both cases, the currents are very weak on the upwind side of the pond and increase moving downstream. Overall, the wind forces a strong convergence zone along the downstream edge with downward vertical velocity along the downstream wall (not shown). Consequently, melting fluxes are highest along the down wind edge of the pond with values of ~300 500 W m^{-2} as shown in Fig. 3a. In contrast, the upwind ice edge has flux values below ~200 W m^{-2}.

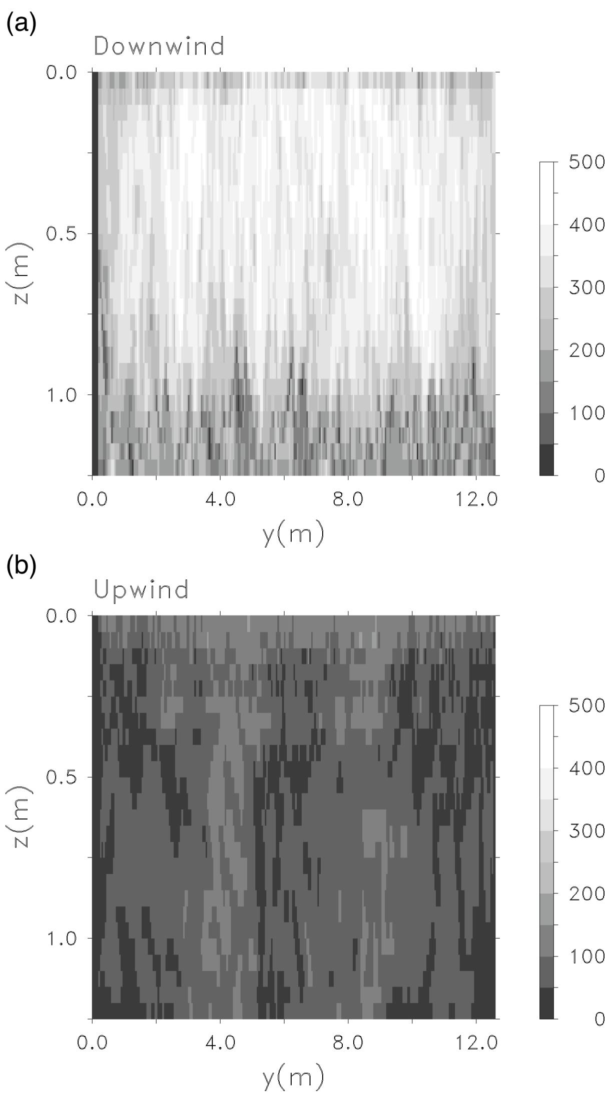

Figure 3. Melting heat fluxes (W m^{-2}) along the (a) downstream and (b) upstream pond edges for the large pond case.

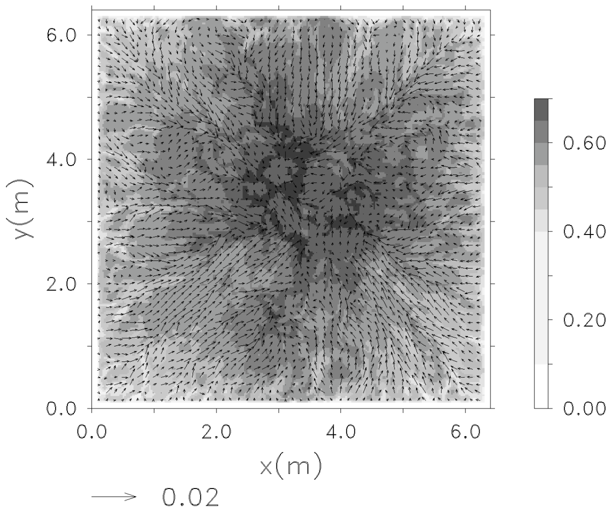

Figure 4. Temperature (^{o}C) and current vectors (m s^{-1}) for the no wind, small lead case.

In the no wind case, currents are much weaker and show a pattern of convergence in pond center with upwelling along the edge of pond (Fig. 4). Temperatures in the pond are very near the freezing point, which results in a density decrease as the water cools. Consequently, water along the pond edges has relatively low density, forcing convective instability and rising water. Water warmed by solar heating converges in the center of the pond and sinks. Edge melting fluxes in this case (Fig. 5) are uniform around the pond edge, with values somewhat larger than the upwind values of the wind driven case, but much lower than the downwind values shown in Fig. 3a.

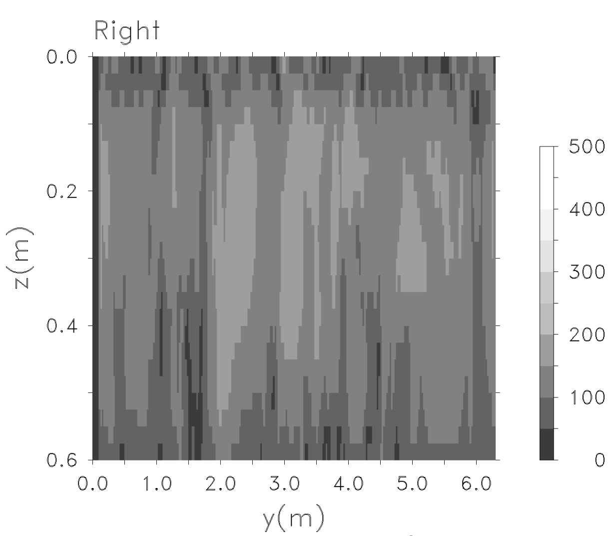

Figure 5. Melting heat flux (W m^{-2}) along the right edge of the no wind case pond.

Heat flux values from the three simulations are presented in Fig. 6. In each case, the melting rates begin with large oscillations as the model flow fields accelerate to near steady state. Fluxes then indicate more gradual change, depending on how close the initial state was with respect to thermal equilibrium.

These plots show that side melting rates are typically slightly larger than the bottom rates. For the small pond, the model shows that wind stress forcing has very little impact on the side wall melting rates with both wind and no wind rates settling at a value of about 110-120 W m^{-2}. Bottom melt rates, however, are strongly affected by wind forcing, with the wind forced case showing a flux of about 90 W m^{-2} in comparison with a flux of ~60 W m^{-2} for the no wind case.

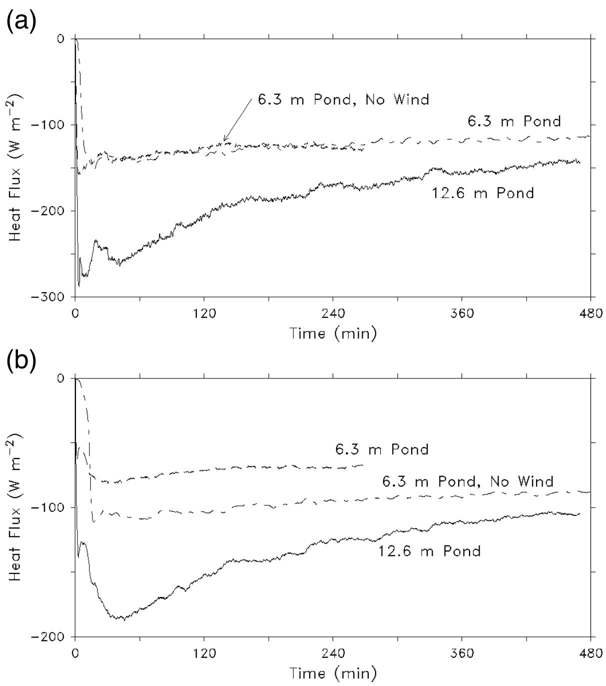

Figure 6. Average melting flux on the (a) pond sides and (b) pond bottom.

Increased pond size generally produces higher melt fluxes as should be expected since there is more water in the pond absorbing solar radiation. Large pond side melting is about 150 W m^{-2}, versus a bottom melting rate of ~100 W m^{-2}.

Overall, the side and bottom melt rates are not equal in the simulations. Consequently, the simple ratio defined by (2) should not be expected to apply in the present cases. In fact, using the average of the side and bottom melt yields a simulated F_r/F_s ~ 0.62 in the small pond with winds, ~0.5 in the small pond without winds, and 0.77 for the large pond case.

We note that the preliminary cases shown here are for ponds with relatively large aspect ratio, d/L ~0.1, in comparison with the observed lead presented above where d/L ~ 0.04. The relatively shallow depth of the observed ponds may force a more constant melting rate as was assumed in (2). Future experiments are planned to explore the role of melt pond geometry on melting rates and determine if simplified melt pond models, for example as present in (1), can adequately represent melt pond characteristics.

4. Conclusions

Preliminary LES simulations of melt ponds indicate that wind driven circulations have a significant impact on the melting rates along the pond wall and bottom. Water movement forced by the wind generates large melting fluxes along the downstream edge of the pond with relatively small fluxes along the upwind edge. Based on the model results, use of a constant melting flux is a poor assumption for melt ponds with characteristic aspect ratios of ~0.05.

5. References

Perovich, D. K., T. C. Grenfell, J. A. Richter-Menge, B. Light, W. B. Tucker III, and H. Eicken, 2003: Thin and thinner: Sea ice mass balance measurements during SHEBA, *J. Geophys. Res.*, 108, 10.1029/2001JC001079.

Skyllingstad, E. D., C. A. Paulson, and W. S. Pegau, 2004: Simulation of turbulent exchange processes in summertime leads. *J. Geophys. Res.*, In press.

Untersteiner, N., 1990, Structure and dynamics of the Arctic Ocean ice cover. In: Grantz, A., Johnson, L., and Sweeney, J. F. (eds) The Arctic Ocean region, pp. 37-51, Boulder, Colorado, Geological Society of America.